Chaotic scattering through potentials with rainbow singularities

Kai T. Hansen* and Achim Kohler†
Fakultät für Physik, Universität Freiburg, Hermann-Herder-Strasse 3, D-79104 Freiburg, Germany
(Received 17 June 1996)

We investigate chaotic scattering in a family of two dimensional Hamiltonian systems. The potential in which a point particle scatters consists of a superposition of a finite number of central force potentials. Each central force potential is either attracting without any singularity, or attracting at long distances with a repelling singularity in the center motivated by potentials used in molecular interaction. The rainbow effect obtained from scattering in one such potential causes the chaotic scattering, and we show that for these systems there exist regions in the parameter space where the repelling sets are complete two dimensional Cantor sets of different type. We define symbolic dynamics and calculate periodic orbits for these systems and determine the classical escape rate and the quantum mechanic resonances using the zeta-function formalism. We examine the systems with two, three, and four attracting Gaussian potentials and two Lennard-Jones potentials.
[S1063-651X(96)11412-4]

PACS number(s): 05.45.+b, 03.80.+r

I. INTRODUCTION

Chaotic scattering is a problem that has received much interest in the last decade. The structure of classical trajectories in these scattering problems has been investigated and quantum mechanical scattering using both semiclassical methods and exact quantum mechanics methods has been examined. The most popular models have been billiard problems, where a particle moves on a two-dimensional plane and bounces elastically from some number of walls. The Lorentz gas [1] and the Sinai billiard [2] are infinite systems of this type. A model for chaotic scattering in a finite region and then escaping was introduced by Eckhardt; the *three-disk system*, where the particle scatters from the borders of three disks in the plane. This may be the simplest physical example of a chaotic scatterer and is the subject of a number of investigations [3–8]. For sufficiently separated disks the chaotic repellor has a complete Cantor set structure, which simplifies the classical and semiclassical discussion. The hard disks in this problem can be replaced by smooth repelling potentials [9], and this model can also give a similar type of chaotic repellor.

Attracting potentials may also yield a chaotic scatterer and an example for a scatterer of this type has been introduced by Troll and Smilansky [10,11]. This system consists of an infinite array of potentials with a finite range where the potentials do not overlap each other and each potential changes the direction of the particle in a linear way. This model yields a repellor with a Cantor set structure. Scattering through a double well potential has been studied by Daniels, Vallières, and Yuan [12] and their system shows some similarities with the systems described below. This paper describes the cases where the double well types of potentials has a Cantor set structure. The symbolic dynamics we introduce must be the starting point for defining symbols also for not complete repellors of this type. The symbolic dynamics introduced in [12] does not distinguish different orbits and cannot be used to label periodic orbits.

In a chaotic system there are two mechanisms acting on trajectories: a dispersing mechanism of neighboring trajectories giving a sensitive dependence on initial conditions and a folding of trajectories that have moved far away from each other such that they again move close. In attracting potentials we may obtain this dispersing and folding mechanisms from the well known rainbow effect in a central force potential [13]. A central force potential that is attracting without an attracting singularity or a potential attractive for large distances and repulsive for short distances has a deflection function such that more than one incoming trajectory (impact parameter) yields the same reflected angle of the particle (deflection angle). This gives the folding of trajectories. Trajectories sufficiently far away from the extremum value of the deflection function have the property that neighboring trajectories disperse and then give the sensitive dependence on initial conditions. A combination of two or more such central force potentials may therefore give rise to chaotic scattering. As we show below this analysis is also valid for composed potentials where the different central potentials overlap. The extremum point of the deflection function creates bifurcations and stable orbits in these systems.

We discuss here model systems, each consisting of a potential that is a superposition of a finite number of central attracting potentials with and without a repelling singularity. The potentials are apparently similar to the three-disk repellors but the repelling set has a different and much richer structure. We show that for certain areas in the parameter space we can obtain a repellor with a simple Cantor set structure, and we discuss the transition between these simple repellors. We introduce a symbolic dynamics to enumerate the orbits and give methods to find orbits numerically. For the simple repellor cases we calculate classical escape rates using the thermodynamical zeta function and we make some

*Present address: NORDITA, Blegdamsvej 17, DK-2100 Copenhagen Ø, Denmark. Also at Physics Department, University of Oslo, Box 1048, Blindern, N-0316 Oslo, Norway. Electronic address: k.t.hansen@fys.uio.no
†Electronic address: ako@phyc1.physik.uni-freiburg.de

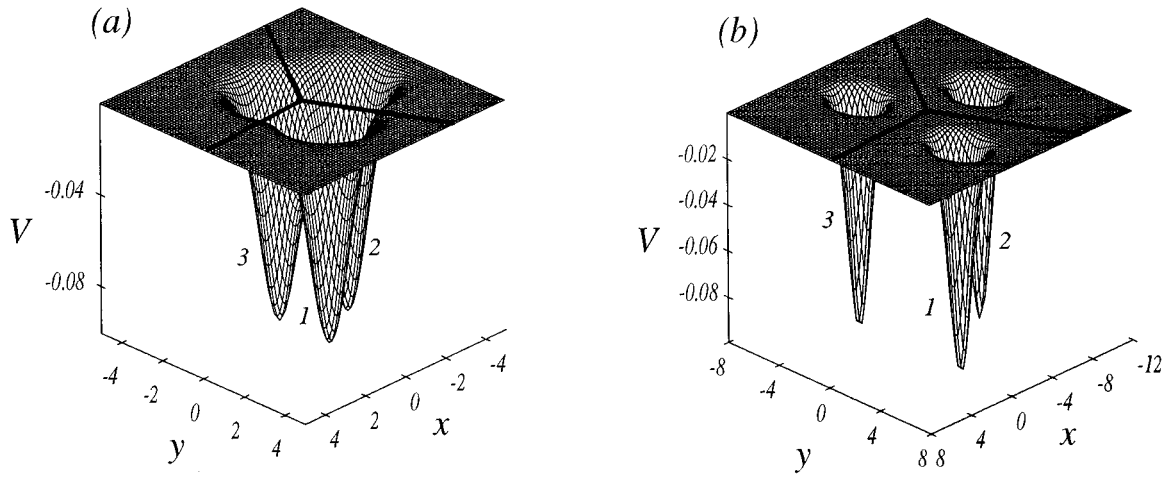

FIG. 1. The three-Gaussian potentials in the (x,y) plane with parameters $V_0=0.1$, $a=1$, and (a) $R=2.5$, (b) $R=8.0$.

semiclassical calculations and obtain quantum mechanical resonances.

This model is motivated by problems in atomic and molecular physics where attracting potentials of this type are typical. A repellor consisting of only attracting Coulomb potentials yields a completely different system [14] and it is essential for our discussion that we have a potential without an attractive singularity. We have chosen Gaussian potentials for the attracting case and Lennard-Jones potentials for the singular scatterer, but other potentials with a similar structure will not change much in our results. The main result we want to focus on is the topological structure of the chaotic scatterer, which in many cases does not depend sensitively on the exact shape of the potential.

II. DEFINITIONS

The Hamiltonian describing the motion of a particle on a plane is

$$H=\frac{p_x^2}{2m}+\frac{p_y^2}{2m}+V(x,y), \tag{1}$$

where $V(x,y)$ may be a smooth function or for billiard systems a discontinuous function of x and y. We choose $V(x,y)$ to be a superposition of some finite number of attractive Gaussian potentials

$$V_i(x,y)=-V_0\exp\left(-\frac{(x-x_i)^2+(y-y_i)^2}{a^2}\right) \tag{2}$$

or Lennard-Jones potentials with a repelling singularity

$$V_i(x,y)=\frac{A_0}{[(x-x_i)^2+(y-y_i)^2]^6}-\frac{B_0}{[(x-x_i)^2+(y-y_i)^2]^3}. \tag{3}$$

When we let a particle pass through one such potential we obtain a deflection function with a rainbow effect for some outgoing angle. It turns out to be essential to control the trajectory moving along the path giving the rainbow singularity and we will refer to this trajectory as a *singular orbit* through the Gaussian or Lennard-Jones potential. Controlling all such singular orbits yields the method to control the topological structure of the chaotic repellor.

We obtain the symmetric three-Gaussian system by choosing three potentials (2) with (x_i,y_i) as the corners of a regular triangle with distance R between the centers $x_1=x_2=y_3=0$, $x_3=-\sqrt{3}R/2$, $y_1=-R/2$, $y_2=R/2$. The parameters of the system are R, V_0, a, m, and E. We will assume below, if not otherwise stated, that $a=m=1$ and $V_0=0.1$. We have chosen this as our main example and most numerical results are given for this system. This example illustrates the general techniques we use and new examples can be worked out using the same methods.

In Fig. 1 the three-Gaussian potential is drawn for two different distances, R, between the disk centers. In Fig. 1(a) the distance is small, $R=2.5$, and the three potentials form one big well with three minimum points. In Fig. 1(b) the potential consists of three separated wells with $R=8.0$. Even if the potentials look very different the dynamics may have the same topological structure choosing a proper energy, and since the latter system is simpler to analyze we will start the discussion in the asymptotic limit $R/a\gg 1$ where the three Gaussian potentials are far from each other and the particle moves nearly as a free particle between two Gaussian wells. To simplify the discussion we enumerate the three Gaussians counterclockwise as indicated in Fig. 1 and denote them Gaussian 1, Gaussian 2, and Gaussian 3.

A two-Gaussian system is similarly defined with $x_i=0$ and $y_i=\pm R/2$ and we have also studied a four-Gaussian system with $x_i=\pm R/2$ and $y_i=\pm R/2$. We investigate the two Lennard-Jones Hamiltonians with $x_i=0$ and $y_i=\pm R/2$. Figure 2 shows this potential for the parameters $A=1$, $B=3$, and $R=10$.

III. ASYMPTOTIC CANTOR SET REPELLORS

To discuss the limit $R/a\gg 1$ we assume that each single potential vanishes at a distance $b_{\max}<R/2$ from the center of the potential. This is practically true for the parameters we have used in Fig. 1(b). Then the particle moves freely between the single potentials and we can investigate the motion through one single Gaussian potential independent of the other Gaussians. The scattering through a single Gaussian is

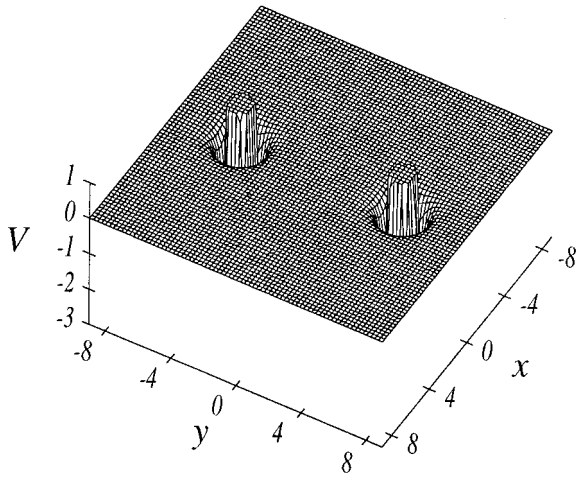

FIG. 2. The two Lennard-Jones potentials in the (x,y) plane with parameters $A_0=1$, $B_0=3$, and $R=10$.

described by finding the deflection angle as a function of the impact parameter [13]. In Fig. 3 the deflection angle is given for $E=0.024$ and the deflection angle reaches a maximum or minimum value $\pm\phi_c$ for some critical impact parameter $\pm b_c$ where the cross section becomes infinite. As the energy decreases this maximum (minimum) value increases (decreases). We restrict our discussion to energies where this maximum value remains finite.

We want to study the classical chaotic scattering and for the quantum mechanical system only describe the resonances. We are therefore not directly interested in the cross section itself [15], but only in the part of the cross section that hits a new attracting potential. Only trajectories in this part can give contributions to the chaotic dynamics and to resonances in the quantum mechanical system. The cross section will change a lot with the incoming angle while the resonances are fixed quantities independent of the direction. Which impact parameters give trajectories remaining in the system depends on the position of the potentials in the plane, on ϕ_c, which is a function of the energy E, the mass m, and the parameters of the potential, V_0 and a.

If a trajectory along the critical deflection angle ϕ_c reaches a new potential, then there is a possibility to have stable orbits and a complicated system. We will therefore first investigate the case where a trajectory along ϕ_c escapes immediately from the system.

A. 2×2 Cantor set

For the three-Gaussian system in Fig. 1(b) with ϕ_c well below 120° there are no trajectories that are captured in the system. Any particle from outside or starting somewhere inside the system will escape as a free particle after having scattered in at most two Gaussian potentials.

The situation is very different if we choose a smaller energy such that ϕ_c is somewhat larger than 120° (the exact value is discussed below) but well below 180°, for example, Fig. 3 with $\phi_c\approx 150°$.

First we make a simplified discussion to illustrate this; let a trajectory from Gaussian 1 in Fig. 1(b) scatter counterclockwise in Gaussian 2 and obtain a deflection angle such that it reaches Gaussian 3. The critical trajectory that scatters counterclockwise with the angle ϕ_c will bend more and pass somewhere between the Gaussian 1 and Gaussian 3 where the potential is 0, and will consequently then escape as a free particle. There are two intervals of the impact parameter b in Fig. 3, one on each side of the critical impact parameter b_c, in which trajectories hit Gaussian 3 and can continue scattering in the system. This creation of these two intervals is the essential point. We can now repeat the same argument for the trajectories in each of these two intervals; in each interval there will be one critical trajectory counterclockwise through Gaussian 3 escaping between Gaussian 1 and Gaussian 2 and two intervals reaching Gaussian 1. We have then obtained four intervals in our initial positions of trajectories from Gaussian 1 and all trajectories in these intervals scatter in Gaussian 2 and Gaussian 3 and return to Gaussian 1. Repeating this argument infinitely many times we get a Cantor set of trajectories remaining in the system forever. The orbits will be unstable as long as the slope for the function in Fig. 3 is sufficiently steep in the relevant intervals of b.

The argumentation above gives the correct idea of the dynamics, but our system is a Hamiltonian with two degrees of freedom and has to be discussed in a two dimensional Poincaré map. It is natural to choose a Poincaré map reflecting the symmetry of the problem and we choose as a Poin-

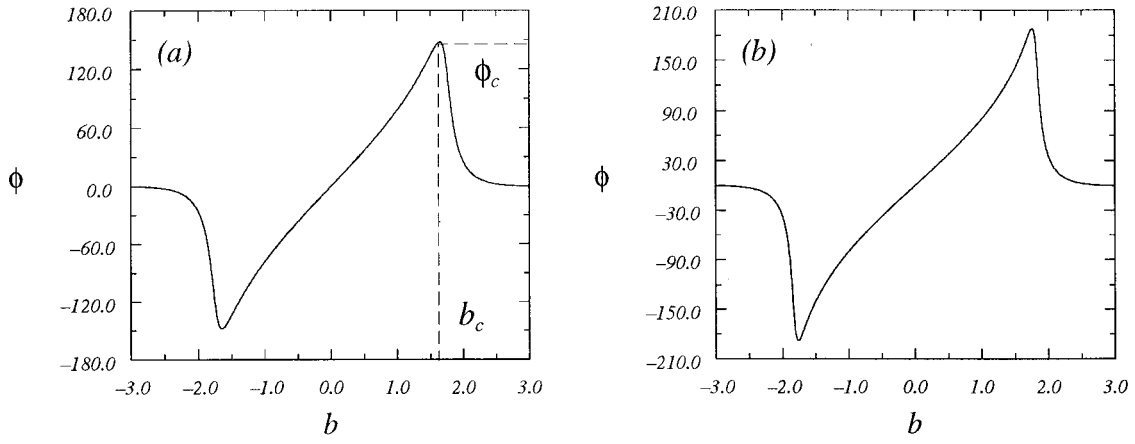

FIG. 3. The deflection angle ϕ in degrees as a function of the impact parameter b for one single Gaussian potential (2) for $a=1$, $V_0=0.1$ and the energy $E=0.024$.

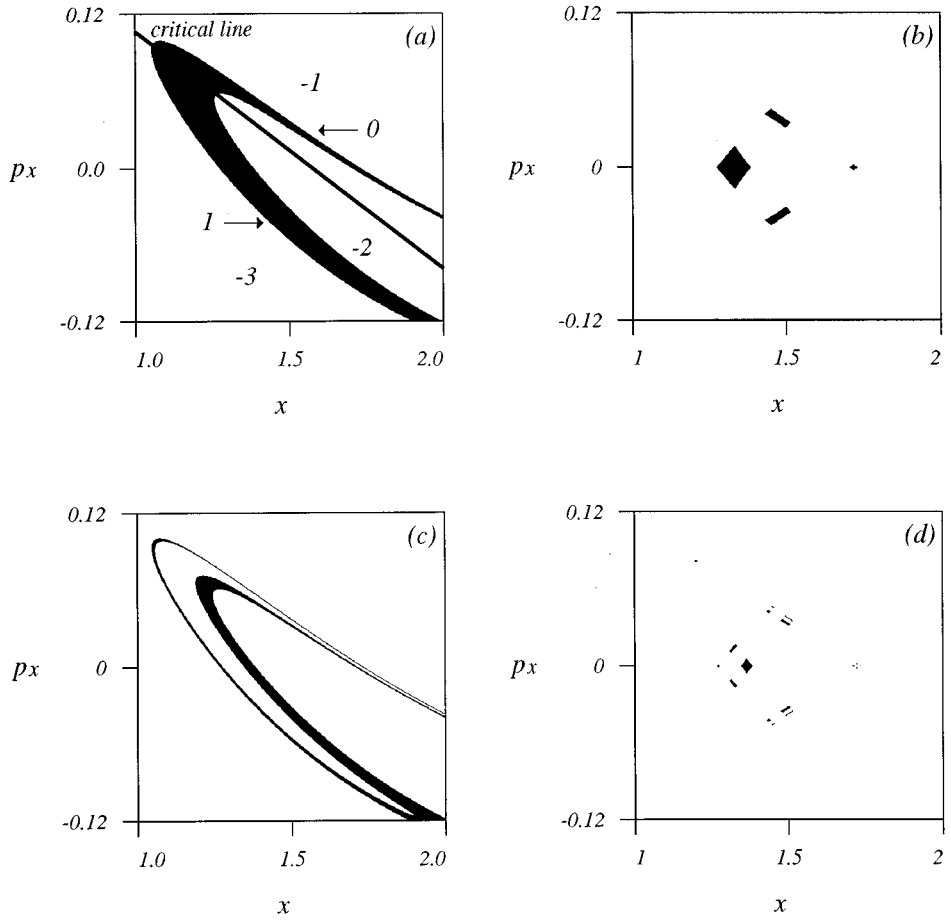

FIG. 4. Starting points of the three-Gaussian system, which remain in the system after some number of scatterings in Gaussian potentials, $E=0.024$, $R=2.5$. (a) One scattering forward in time (Smale horseshoe), (b) one scattering forward and one scattering backward, (c) two forward, and (d) two forward and two backward. In (a) the symbolic dynamics s_t is indicated.

caré map the crossing of the trajectory with one of the lines from the midpoint in the triangle $x=0$, $y=0$ going between any two Gaussians; that is the three lines indicated in Fig. 1, $y=0$ for $x>-R/\sqrt{12}$, $y=\pm(\sqrt{3}x+R/2)$ for $x<-R/\sqrt{12}$. As the abscissa in this Poincaré map we choose the position on the symmetry line, which we denote for simplicity also by x and set $x=0$ at the midpoint between two Gaussians and as the ordinate we choose the momentum in this x direction, p_x.

As a numerical experiment we scan the starting points of the Poincaré plane and plot only the points that scatter at Gaussian 1 and then arrive close to Gaussian 2. This is done in Fig. 4(a) and we find an area similar to the well known Smale horseshoe map [16]. In the Poincaré plane there is one connected curve of starting points yielding the critical deflection in the first Gaussian as indicated in Fig. 4(a), and these give the primary turning points of the horseshoe folding in the asymptotic limit. To construct the two dimensional Cantor set we also have to follow the trajectories backward in time. In Fig. 4(b) the points reaching a Gaussian after having scattered both once forward in time and once backward in time are plotted, and we get four areas, which are called rectangles, in the Poincaré plane.

What is important here is that there are always critical trajectories from the Poincaré plane reaching a new Gaussian but only forward in time or only backward in time. There is no point giving a critical trajectory reaching a new Gaussian both forward and backward in time; the trajectory scattering along a critical trajectory forward in time will escape backward in time and visa versa. This is the essential part in our construction of the Cantor set repellor.

To get the next generations in the construction of the Cantor set repellor we just repeat the argument for each of the four rectangles in Fig. 4(b), scattering twice forward and twice backward yields 16 rectangles. In Fig. 4(c) we have drawn the points not escaping after two iterations forward in time. This yields a twice folded horseshoe. In Fig. 4(d) the 16 rectangles of orbits not escaping after two scatterings forward and backward in time are drawn. Three scatterings yield 64 rectangles and so on. In the limit $R\to\infty$ the repellor has this topological structure for $120°<\phi_c<180°$. We will refer to this repellor as the 2×2 *Cantor set.*

A *symbolic dynamics* description of the Cantor set is determined by labeling a point in the Poincaré plane in the upper right fold of the horseshoe in Fig. 4(a) $s=0$, and in the lower left fold $s=1$ as indicated in the figure. Then $s=1$ corresponds to the fact that the particle will be scattered in the next Gaussian along a trajectory closer to the center of the Gaussian than the critical trajectory and we call this an *inner bounce*. For $s=0$ we have an *outer bounce*, a trajectory outside of the critical trajectory. Any trajectory in the repellor is uniquely determined by a bi-infinite symbol string

$$\cdots s_{-1}s_0\cdot s_1s_2\cdots, \quad s_t\in\{0,1\} \tag{4}$$

where the symbols to the right and to the left of the dot describe the scattering forward and scattering backward in time. We use the convention that a line above a symbol string denotes an infinite repetition of the string. Periodic orbits are written as $\overline{s_1s_2\cdots s_n}=(s_1s_2\cdots s_n)^\infty$.

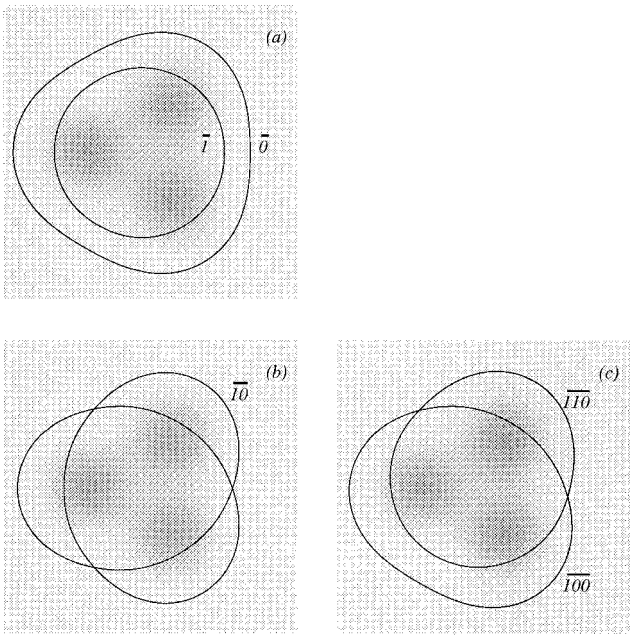

FIG. 5. Periodic orbits of the three-Gaussian system in the full configuration space. (a) $\overline{0}$ and $\overline{1}$, (b) $\overline{10}$, and (c) $\overline{110}$ and $\overline{100}$.

The orbits discussed here are always moving counterclockwise around the center of the system. In addition we have orbits moving clockwise close to the minimum of the deflection function in Fig. 3. As long as a trajectory cannot turn and retrace its own path two different trajectories always exist related by a time reversing symmetry. We then also have a Cantor set of orbits moving in the opposite direction.

The symmetric three-Gaussian repellor has the symmetry C_{3v} and the dynamics can be reduced to the dynamics in 1/6th of the configuration space, *the fundamental domain*, with suitable group transformations as discussed by Cvitanović and Eckhardt [17]. The symbolic dynamics we use here [Eq. (4)] actually describes the dynamics in the fundamental domain. This reduction to the fundamental domain simplifies the calculations and improves the convergence of the zeta function calculations.

Some simple periodic orbits are drawn in Figs. 5 and 6. The length of the orbit is different in the fundamental domain, Fig. 6, and in the full domain, Fig. 5. The period 1 orbits with symbolic description $\overline{0}$ and $\overline{1}$, Fig. 5(a), and the period 3 orbits $\overline{100}$ and $\overline{110}$, Fig. 5(c), all are closing after one complete loop in the full configuration space while the period 2 orbit $\overline{10}$, Fig. 5(b), is closing after two loops in the full space. Table I lists the shortest periodic orbits of this repellor.

B. Other Cantor set repellors for the three Gaussian

The critical deflection angle ϕ_c of a single potential increases when the energy decreases. If the critical deflection angle ϕ_c is somewhat larger than 180° but well below 240° we obtain a different repellor. The trajectory from Gaussian 1 scattering counterclockwise along ϕ_c in Gaussian 2 will end between Gaussian 1 and Gaussian 2 and escape. The trajectory from Gaussian 1 may also scatter clockwise

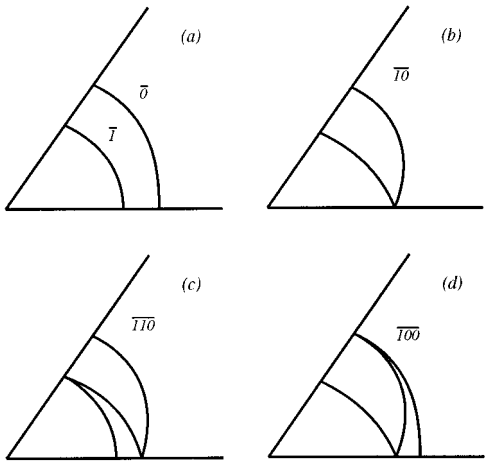

FIG. 6. Periodic orbits of the three-Gaussian system in the fundamental domain. (a) $\overline{0}$ and $\overline{1}$, (b) $\overline{10}$, (c) $\overline{110}$, and (d) $\overline{100}$.

along ϕ_c in Gaussian 2 and arrives between Gaussian 1 and Gaussian 3 and escapes. There are then six different intervals of the impact parameter, which yields trajectories remaining in the system; one inner and one outer orbit bouncing counterclockwise in Gaussian 2 reaching Gaussian 3, one inner and one outer orbit bouncing counterclockwise in Gaussian 2 reaching Gaussian 1, and one inner and one outer orbit bouncing clockwise in Gaussian 2 reaching Gaussian 1.

The two dimensional discussion proceeds as above and we obtain $6\times6=36$ rectangles in the Poincaré map for orbits scattering at least one time in the future and at least one time in the past. Symbolic dynamics is then defined with six symbols and all orbits in the repellor are described using

$$\cdots s_{-1}s_0\cdot s_1s_2\cdots, \quad s_t\in\{0,1,\ldots,5\} \tag{5}$$

in the fundamental domain. Two of these symbols can be identified with the two symbols in the 2×2 Cantor set repel-

TABLE I. The logarithm of the stability Λ_p, the action S_p, the time T_p, and the Maslov index m_p for the shortest periodic orbits in the binary three-Gaussian repellor for $E=0.016$ and $R=2.5$.

Periodic orbit	$\ln(\Lambda_p)$	S_p	T_p	Maslov index
$\overline{1}$	1.21324	1.33609	14.16627	1
$\overline{0}$	4.54595	1.22159	30.24667	0
$\overline{10}$	5.53465	2.60128	41.13907	1
$\overline{110}$	6.90987	3.92496	56.61924	2
$\overline{100}$	10.15363	3.82353	71.46064	1
$\overline{1110}$	8.07331	5.26475	70.36953	3
$\overline{1100}$	11.49029	5.14687	86.90523	2
$\overline{1000}$	14.70092	5.04513	101.70902	1
$\overline{11110}$	9.30549	6.59974	84.67796	4
$\overline{11100}$	12.66306	6.48675	100.66375	3
$\overline{11010}$	12.45185	6.52629	97.76407	3
$\overline{11000}$	16.03689	6.36847	117.15278	2
$\overline{10100}$	15.68763	6.42480	112.59887	2
$\overline{10000}$	19.24689	6.26672	131.95572	1

lor while the other four symbols describe orbits created in bifurcations as the energy decreases.

It can easily be seen that if the critical deflection angle ϕ_c is only slightly larger than 180° we may have a different and more complicated repellor. It turns out to be a mixed 2×4 Cantor set repellor.

For limit $R/a \gg 1$ with smaller energies yielding a larger but finite ϕ_c the repellor becomes a Cantor set with an increasing number of rectangles, either with a fixed number of new intervals in each generation or with different numbers. For $240° < \phi_c < 480°$ we get a regular 8×8 Cantor set repellor. As the energy decreases the Cantor set gets larger and we get many more periodic orbits of short lengths.

In the limit decreasing the energy such that ϕ_c goes to ∞ the trajectory can move infinitely many times around one Gaussian before reaching the next, and a Cantor set then would need an infinite number of intervals even in the first generation. In this case there is a stable orbit around one single Gaussian and there do not exist a hyperbolic repellor. Investigating these chaotic systems and systems with $E<0$ is beyond the scope of this paper but we belive an investigation of these systems has to be an extentation of the results obtained here.

C. Asymptotic Cantor set repellors for the two-Gaussian system

The Cantor sets for the two-Gaussian system is in the asymptotic limit a subset of the Cantor sets for the three-Gaussian system. As the Poincaré plane we choose (x,p_x) for $y=0$. In the asymptotic case with a mixed 2 and 4 Cantor set in the three-Gaussian potential we get a 2×2 Cantor set for the two-Gaussian potential. For ϕ_c well above 180° and below 540° the repellor is a 4×4 Cantor set, a subset of the 6×6 or 8×8 Cantor set of the three-Gaussian system. For smaller values of R the topological structure remains the same but the actual orbits are different from the corresponding subset in the three-Gaussian system. A symbolic dynamics with two or four symbols can be applied to describe these two repellors. Larger ϕ_c yields more complicated Cantor sets in the same way as for the three-Gaussian system.

D. Asymptotic Cantor set repellors for the multi-Gaussian system

This way to analyze an asymptotic limit can be generalized to any finite number of Gaussian attractors. For infinite systems with Gaussians on a square lattice it is not possible to get the complete repelling set because there will always be a critical trajectory that does not escape. An approximate description may, however, be possible. The unstable orbits in such a system may have an infinite but countable Markov partition. This kind of lattice for disk systems (Sinai billiard) has been much studied.

E. Lennard-Jones potentials

Including a singular repellor in the center of the potential adds a new possibility of scattering from the single potential but the analysis above to determine the Cantor set can be repeated as the important critical trajectory still is the trajectory through the rainbow singularity. The trajectories bouncing back from the repelling singularity can always reach any other potential as long as the potentials are well separated. One example of a Cantor set repellor for the Lennard-Jones potential is obtained with the parameter values $E=1.9$, $A_0=1$, $B_0=3$, and $R=10$. For these parameters we have in the Poincaré plane $y=0$ a similar repellor as the 4×4 Cantor set for the two-Gaussian system, but in addition an interval with orbits bouncing back from the repelling singularity. This gives us a 5×5 Cantor set repellor, and some short orbits are drawn in Fig. 7. A five-letter symbolic dynamics is defined for this system by labeling each of the five stripes in the horseshoe folding, $s_t \in \{0,1,\ldots,4\}$, where 0 and 1 correspond to outer and inner clockwise bounce, 2 to a bounce from the repelling part, and 3 and 4 to inner and outer anticlockwise bounce. By choosing a 180° rotation each time the trajectory crosses the x axis we have a unique coding for the system in one-half of the configuration space.

TABLE II. The logarithm of the stability Λ_p, the action S_p, and the time T_p for the shortest periodic orbits for the two Lennard-Jones potentials with $E=1.9$ and $R=10.0$.

Fundamental domain	Half plane	$\ln(\Lambda_p)$	S_p	T_p
$\overline{0}$	$\overline{0}$	7.96789	28.83628	6.65926
$\overline{1}$	$\overline{1}$	6.05727	28.89761	6.40678
$\overline{2}$	$\overline{2}$	3.03531	17.03942	4.16773
$\overline{3}$	$\overline{13}$	6.50561	29.69172	6.46975
$\overline{4}$	$\overline{04}$	8.49030	29.65795	6.69145
$\overline{01}$	$\overline{01}$	14.02648	57.73408	13.06570
$\overline{02}$	$\overline{02}$	11.30791	46.32394	10.84308
$\overline{03}$	$\overline{0341}$	14.52473	58.54051	13.11474
$\overline{04}$	$\overline{0044}$	16.48756	58.49467	13.35192
$\overline{12}$	$\overline{12}$	9.34183	46.36862	10.60726
$\overline{13}$	$\overline{1133}$	12.56192	58.58634	12.87756
$\overline{14}$	$\overline{1430}$	14.52473	58.54051	13.11474
$\overline{23}$	$\overline{1232}$	9.31555	46.33053	10.60673
$\overline{24}$	$\overline{0242}$	11.27803	46.28455	10.84410
$\overline{34}$	$\overline{14}$	14.99585	59.34960	13.16142

The fundamental domain is, however, only 1/4 of the full configuration space; $x>0$, $y>0$. We obtain a symbolic coding in the fundamental domain by mapping the trajectory back into the fundamental domain either by a 180° rotation or by a reflection $y\rightarrow -y$ each time the trajectory crosses the x axis, and use this choice to determine the symbol. The fixed points and the period-two orbits are given in Table II, where the symbolic description is given both for the fundamental domain and for the half configuration plane. The orbits in Fig. 7 are labeled by the fundamental domain alphabet.

In the Lennard-Jones system it is possible for an orbit to retrace itself and some orbits are their own time reversal orbits. There is also a periodic orbit labeled $\overline{2}$, which is on the symmetry line $y=0$. This implies a more complicated factorization of the zeta function [17].

IV. WELL ORDERED SYMBOLS

To be able to describe the pruned regions and to numerically find periodic orbits it is useful to define new symbols,

$W=\cdots w_{t-1}w_t w_{t+1}\cdots$, which have an ordering in the same way as the folds of the unstable and the stable manifolds are ordered in the Poincaré plane [18,8,11]. Cvitanović [7] showed that this makes it possible to define a pruning front that describes the nonadmissible orbits in the system. We will also need this symbolic description to calculate periodic orbits.

To define well ordered symbols w_i, we have to determine which part of the horseshoe map preserves the ordering of the manifolds in the Poincaré map from one crossing of the Poincaré plane to the next crossing, and which part of the horseshoe flips the ordering of the manifolds. Two parallel neighboring trajectories bouncing at the outside of the critical trajectory do not cross each other and the ordering through this bounce is conserved. Two trajectories inside of the critical trajectory will cross each other before reaching the next Poincaré plane and therefore flip the ordering in the Poincaré plane. The critical trajectory does not have a well defined conserving or flipping, but as long as this trajectory does escape this does not pose any problems for our discussion. The scattering from the repelling center of the Lennard-Jones potential is like a dispersing bounce that flips the ordering.

In the 2×2 Cantor set repellor for the three-Gaussian system $s_t=0$ corresponds to preserving ordering and $s_t=1$ to flipping the ordering. We define a *future parity* p_t as

$$p_1=\begin{cases} 1 & \text{if} \quad s_1=0 \\ -1 & \text{if} \quad s_1=1, \end{cases}$$

$$p_{t+1}=\begin{cases} p_t & \text{if} \quad s_{t+1}=0 \\ -p_t & \text{if} \quad s_{t+1}=1 \end{cases} \tag{6}$$

and the parity for the past as

$$p_0=\begin{cases} 1 & \text{if} \quad s_0=0 \\ -1 & \text{if} \quad s_0=1, \end{cases}$$

$$p_{t-1}=\begin{cases} p_t & \text{if} \quad s_{t-1}=0 \\ -p_t & \text{if} \quad s_{t-1}=1. \end{cases} \tag{7}$$

We then get the well ordered future symbols as

$$w_1=s_1,$$

$$w_t=\begin{cases} s_t & \text{if} \quad p_{t-1}=1 \\ M-1-s_t & \text{if} \quad p_{t-1}=-1 \end{cases} \tag{8}$$

with $M=2$ and well ordered past symbols by

$$w_0=s_0,$$

$$w_t=\begin{cases} s_t & \text{if} \quad p_{t+1}=1 \\ M-1-s_t & \text{if} \quad p_{t+1}=-1. \end{cases} \tag{9}$$

We can define symbolic values for the future γ and the past δ:

$$\gamma=0.w_1w_2w_3\ldots=\sum_{t=1}^{\infty}\frac{w_t}{M^t},$$

$$\delta=0.w_0w_{-1}w_{-2}\ldots=\sum_{t=1}^{\infty}\frac{w_{1-t}}{M^t}. \tag{10}$$

Corresponding well ordered symbols can in the same way be defined for the more complicated Cantor sets. One simply uses the symbols s_t as obtained from the first folding of the horseshoe and let p_t change sign if the bounce is a bounce that changes the ordering. The integer M is then equal to the number of symbols.

Each point in the (γ,δ) plane corresponds to one nonescaping orbit in the three-Gaussian system. If we choose points along a curve in the Poincaré plane (x,p_x) then γ is defined for each crossing between this curve and the stable manifolds and γ is monotonously increasing as one crosses the consecutive folds. In the same way δ increases monotonously as one crosses the unstable manifolds.

V. PERIODIC ORBITS

We will apply the thermodynamic and semiclassical theory for this scattering problem and have to find the periodic orbits in the system. The standard way of using a Newton method can be applied for this system, but since we have a rather thin Cantor set it is very hard to find a sufficiently good initial guess such that the Newton method converges. It is then difficult to find all the long periodic orbits that we need. Instead we have applied the method introduced in Ref. [19]. This is a systematic search for an orbit with a given symbolic description and is here implemented as a binary search. This method converges slightly slower than a Newton method but fast enough for the applications we consider.

To determine a periodic orbit we iterate an arbitrary starting point in the Poincaré plane and determine its symbolic description. Every time the trial trajectory crosses the Poincaré plane we use the point (x,p_x) to determine the symbol according to Fig. 4(a). In addition to the symbols s_t describing the nonescaping trajectories we introduce three new symbols n_t for the position of a trajectory that will escape from the system. We divide the Poincaré plane into five areas: with symbols 0 and 1 corresponding to the two folds of the horseshoe mapping and three areas in which we know that the trajectory will escape from the system before reaching the next Poincaré map. These three areas are below the horseshoe, between the folds of the horseshoe, and above the horseshoe and we denote them by the symbols -3, -2, and -1. A positive symbol means that a trajectory remains in the system and scatters at least one more time while a negative symbol implies leaving the system. After some iterations the trial orbit hits the Poincaré plane in an area with negative symbolic description and escapes. To find the well ordered symbols we use Eq. (8) as long as the symbols are positive. For the last symbol n_i, which is negative, we apply the following rule:

$$w_t=\begin{cases} -n_t-1 & \text{if} \quad p_{t-1}=1 \\ n_t+M+1 & \text{if} \quad p_{t-1}=-1. \end{cases} \tag{11}$$

Escaping symbols for the past are found in a similar way. What we have done here is extend the ordering of the nonwandering set to those points in the Poincaré plane that do not belong to the Cantor set. The values γ and δ are calcu-

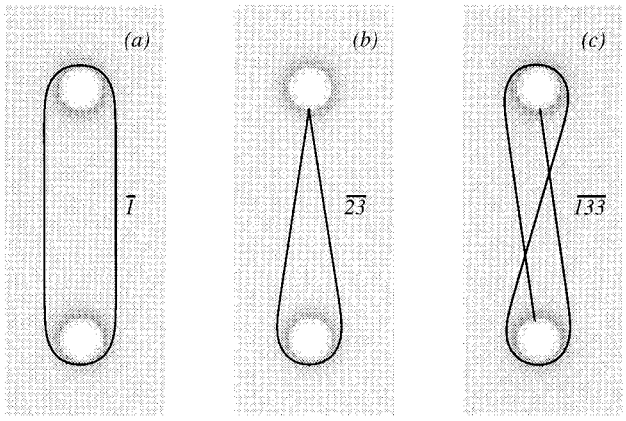

FIG. 7. Some periodic orbits in the Lennard-Jones system in the full configuration space. (a) $\overline{1}$, (b) $\overline{23}$, and (c) $\overline{133}$.

lated as in (10), with the difference that the sum is finite. If we now compare the symbolic values for the trial orbits with the symbolic values for the periodic orbit we want to find, we know in which direction on the Poincaré plane we have to move the starting point. We then implement this search as a two dimensional bisection method.

For each periodic orbit we have calculated the stability Λ_p, which is the largest eigenvalue of the monodromy matrix, the action $S_p = \int p dq$, and the time T_p. For the shortest periodic orbits of the binary repellor for $E = 0.016$ and $R = 2.5$ we have the logarithm of the stability, $\ln(\Lambda_p)$, the action S_p, and the period T_p, all in the fundamental domain, given in Table I.

By using the same kind of method we have determined periodic orbits in the two- and four-Gaussian systems. Also for the two Lennard-Jones potentials we have determined a well ordered symbolic dynamics from the half system symbolic dynamics and determined the periodic orbits. Table II yields the stability, action, and period for the shortest orbits.

VI. BIFURCATIONS IN THE PARAMETER SPACE

We have shown above that for large R the chaotic repellors have different structures for different values of the energy E. The transitions from one repellor to another repellor consist of bifurcations of orbits as we change one of the parameters in the problem. The bifurcations may be global where the unstable and stable manifolds of the Cantor set become tangents or it may be local bifurcations when a stable orbit changes its winding number isolated within a stable island. We are here interested in the global bifurcations because these determine the borders of the parameter areas where we have one Cantor set repellor. We make the assumption that all orbits can be described by a symbolic dynamics string in an alphabet describing a complete Cantor set. If we have a stable orbit this orbit can always be adiabatically followed changing the energy and the distance R until we get a complete Cantor set with a well defined symbolic description.

The exact bifurcation that changes the hyperbolic repellor can be understood by observing the manifolds in the Poincaré map. We will treat the 2×2 Cantor set for the three-Gaussian system in detail and the other repellors can be analyzed in a similar way.

As we have seen above the well ordered symbolic dynamics enumerates each fold of the unstable and stable manifolds such that the rightmost fold is given by a symbol string $W = 0000\ldots$ and the leftmost fold as $W = 1111\ldots$. The 2×2 Cantor set can be destroyed in two ways; either there is a tangent between two manifolds such that we lose orbits from the hyperbolic repellor, or there is a tangent between two manifolds such that new orbits are created. For R sufficiently large, the first bifurcation takes place for a large energy, while the other bifurcates for a smaller energy. For smaller R these two limits may cross each other and then there are no parameter intervals in E with a complete 2×2 Cantor set repellor.

The first bifurcation removing orbits from the Cantor set removes the two homoclinic orbits with symbolic dynamics $S = \overline{0}1110$ and $S = \overline{0}1010$. In the Poincaré map this is the crossing between the leftmost unstable manifold and the innermost fold in the horseshoe of stable manifolds. Both these folds are manifolds from the hyperbolic fixed point $S = \overline{0}$, which is one corner point of the Cantor set. To determine the bifurcations numerically we determine the singular trajectory starting normal to the line $y = \sqrt{3}x + R/2$, $x > 0$, and find the energy when this trajectory has a bifurcation. Figure 8(a)

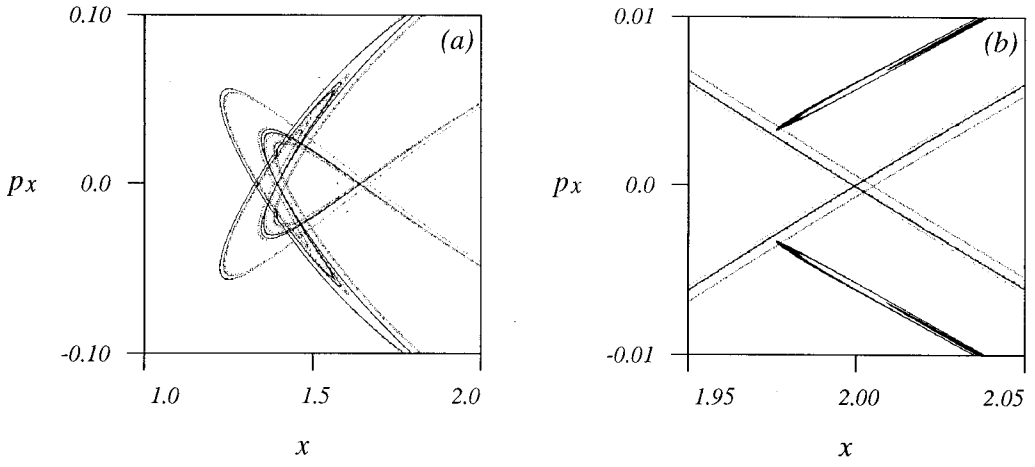

FIG. 8. The manifolds at the bifurcation points of the 2×2 Cantor set repellor for $R = 2.5$. (a) $E = 0.02625$; (b) $E = 0.01369$.

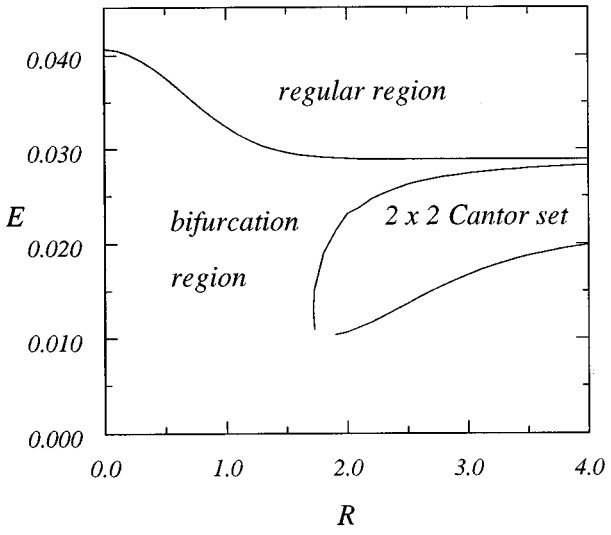

FIG. 9. The bifurcation curves in the plane (R,E) giving the first bounded orbit and the border curves for the simple 2×2 Cantor set repellor, $V_0=0.1$ and $a=1$.

shows the manifolds at this bifurcation point.

The other bifurcation that creates new orbits but does not change the old 2×2 Cantor set takes place when a new fold of the unstable manifold of the fixed point $\bar{0}$ becomes tangent to the stable manifold of this fixed point. A magnification of the manifolds in this bifurcation is drawn in Fig. 8(b). This bifurcation point we get by first finding the singular trajectory normal to the line $y=0$, and then determine the energy where this trajectory has a bifurcation.

We have determined the bifurcation curves in the parameter plane (R,E), and Fig. 9 gives the bifurcation curves that are the borderlines of the areas in the (R,E) plane where we have the 2×2 Cantor set of the three-Gaussian system together with the bifurcation curve where the first bounded orbit starts to exist in the system. For the smallest R values it is difficult to determine numerically the bifurcation point.

The bifurcations and the orbits in the regions between the main Cantor set areas can be examined by investigating the stable and unstable manifolds. Figures 10(a)–10(c) show the manifolds as one changes the parameters in the area between the 2×2 area and the mixed-4×2 area. The manifolds move through each other, and Fig. 10(d) is a Poincaré map for parameter values between Figs. 10(b) and 10(c) showing that there is a stable periodic orbit surrounded by an island with KAM (Kolmogorov-Arnold-Moser) tories as expected for bifurcations of this type. Since the tangent points are created by the rainbow singularity, we can consider the stability of such a stable orbit to be given by this rainbow singularity where nearby trajectories may converge to each other.

The unstable orbits in the not complete repellor case can in principle be described by a pruning front in the symbol plane (γ,δ). We then first have to determine symbolic dynamics for the orbits and one may do this by defining a partition curve through the primary turning points, following the idea of Grassberger and Kantz who used this kind of partition for the Hénon map [20]. From this pruning front it will be possible to construct a Markov description of the dynamics, either exact if one exists, or an approximation [21].

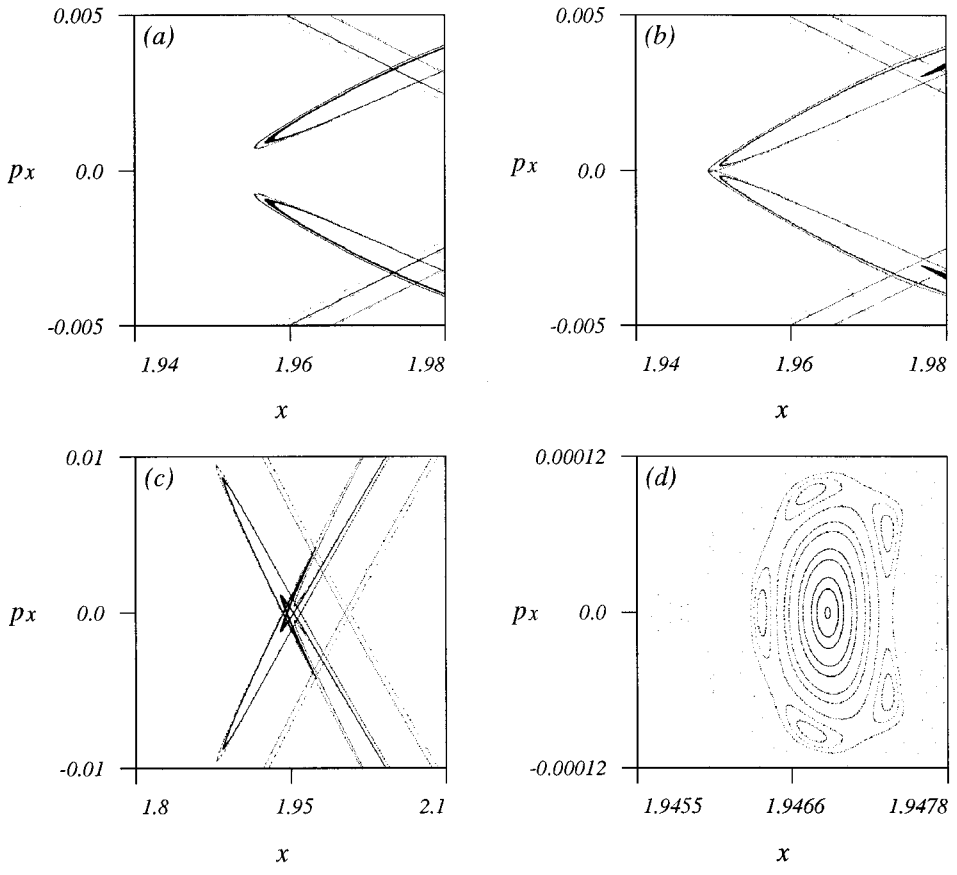

FIG. 10. The manifolds as one changes the parameters in the area between the 2×2 area and the mixed 4×2 area, $R=2.5$. (a) $E=0.013675$, (b) $E=0.013670$, (c) $E=0.013600$, and (d) Poincaré map showing a stable island $E=0.013620$.

TABLE III. The escaperates for the three-Gaussian binary repellor for different parameter values using the cycle expansion up to the given length.

E	R	Length 1	Length 2	Length 3	Length 4
0.016	2.3	0.07274	0.07189	0.07301	0.07265
0.016	2.5	0.07740	0.07758	0.07795	0.07784
0.017	2.5	0.07788	0.07743	0.07800	0.07785
0.017	2.6	0.07953	0.07943	0.07978	0.07969
0.017	2.8	0.08176	0.08209	0.08220	0.08218
0.018	2.5	0.07796	0.07681	0.07762	0.07740
0.018	2.7	0.08096	0.08053	0.08091	0.08082
0.018	2.9	0.08268	0.08264	0.08281	0.08278
0.018	3.1	0.08350	0.08367	0.08374	0.08373

VII. ESCAPE RATES

The classical escape rate can be calculated for chaotic repellors by using the thermodynamic formalism with dynamical ζ functions. This is discussed in Refs. [22] and [7]. With $t_p = e^{\gamma T_p}/|\Lambda_p|$ where p is the label of a primary periodic orbit, T_p is the period of the orbit, and Λ_p is the stability of the orbit, we find the escape rate γ from the zero points of the function:

$$\begin{aligned} 1/\zeta = 1 - t_0 - t_1 - [(t_{01} - t_1 t_0)] - [(t_{001} - t_{01} t_0) \\ + (t_{011} - t_{01} t_1)] - [(t_{0001} - t_0 t_{001}) + (t_{0111} - t_{011} t_1) \\ + (t_{0011} - t_{001} t_1 - t_0 t_{011} + t_0 t_{01} t_1)] - \cdots \\ = 1 - \sum_f t_f - \sum_n c_n . \end{aligned} \tag{12}$$

In Eq. (12) we get two contributions, which are called *fundamental* terms t_f and *curvature* terms c_n. The fundamental terms are large and have to be included in the calculations. The curvature terms are constructed such that each c_n [corresponding to a square bracket in Eq. (12)] includes a shadowing effect and the term is relatively small. The terms c_n decrease fast with the length n and we include only c_n up to a given maximum value of n. In Table III some results are given for the region of the chaotic binary repellor in the three-Gaussian system. The escape rates are calculated for different cycle lengths n. We have done this up to cycle length $n=4$ and it converges fast. Table IV contains some results for the binary repellor of two Gaussians and Table V for the Lennard-Jones potential where we have used a similar expansion of the ζ function with five symbols.

TABLE IV. The escaperates for the two-Gaussian binary repellor for different parameter values using the cycle expansion up to the given length.

E	R	Length 1	Length 2	Length 3	Length 4
0.016	2.5	0.09073	0.09062	0.09063	0.09063
0.017	2.5	0.09012	0.08971	0.08977	0.08976
0.018	2.5	0.08788	0.08708	0.08719	0.08717

TABLE V. The escape rates for the two Lennard-Jones potentials.

E	R	Length 1	Length 2
1.9	10	0.646989	0.648509

Escape rates can also be found by performing a numerical experiment. The escape rate γ is given by the exponential decay of the number of trajectories remaining in the system. We limit the system by making a border that is a circle containing the chaotic repellor where the center of the circle coincides with the center of the system. The exponential decay can be calculated by starting a lot of trajectories randomly and computing the flight time until the trajectory leaves the system. We have done this in Fig. 11 for a binary repellor of the three Gaussians and in Fig. 12 for the Lennard-Jones potential in the case where the chaotic repellor forms a 5×5 Cantor set. The slope of the straight line drawn here is given by the escape rate gained by evaluating the ζ function. The escape rates agree to the precision we get for γ for the numerical experiment. This gives a numerical check of our ζ-function calculations.

VIII. SEMICLASSICAL CALCULATIONS

Scattering potentials exhibiting rainbow singularities are generic in atomic physics and we now want to demonstrate how semiclassical resonances can be found [22,23]. We investigate the case in which the three Gaussians form a binary chaotic repellor. Other chaotic repellors can be treated in the same way.

We consider the system of three Gaussians when the chaotic repellor forms a 2×2 Cantor set. This is true for the energy range $E \in [0.016, 0.0247]$, for $R=2.5$. In this case the symbolic description is complete with the alphabet $\{0,1\}$.

We have for the semiclassical calculations the same expansion as in (12) but with a different t_p;

$$t_p = \frac{e^{(i/\hbar)S_p(E) - i\pi m_p/2}}{|\Lambda_p|^{1/2}}, \tag{13}$$

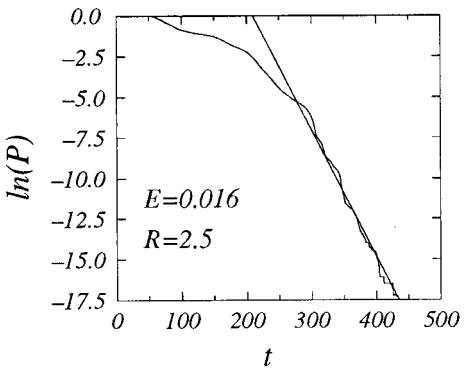

FIG. 11. Exponential decay of the trajectories in the three-Gaussian system, $E=0.016$, $R=2.5$. The slope of the straight line is taken from Table III.

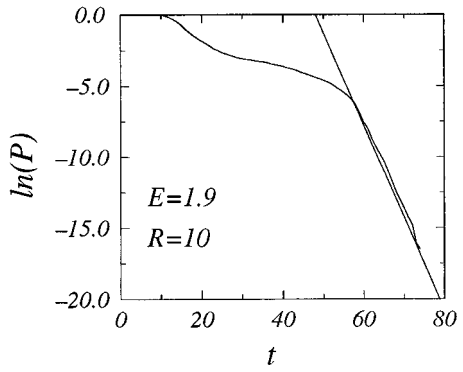

FIG. 12. Exponential decay of the trajectories in the two Lennard-Jones system, $E=1.9$, $R=10.0$. The slope of the straight line is taken from Table V.

where $S_p(E)$ is the classical action and m_p is the Maslov index.

In a system of two degrees of freedom the Maslov index is twice the number of times the stable and unstable manifolds wind around the periodic orbit [24]. In the chaotic binary repellor this number depends on the symbolic dynamics in a simple way. Scattering outside the critical line ($s_t=0$) means that neighboring trajectories conserve their orientation, the stable and unstable manifold do not wind around the periodic orbit. Scattering inside the critical line ($s_t=1$) means neighboring trajectories change their orientation, the stable and unstable manifold wind half around the periodic orbit. The Maslov index m_p for a periodic orbit of length n with the symbolic $s_1,s_2,\ldots,s_n$ is then

$$m_p=\sum_{i=1}^{n} s_i . \tag{14}$$

In chaotic systems like the hydrogen atom in magnetic field [25] and the collinear helium atom [26] are $S_p(E)$ and $\Lambda_p(E)$ energy scaling functions. It is sufficient to calculate the periodic orbit and $S_p(E)$ and $\Lambda_p(E)$ for one parameter value of E and then use scaling relations to obtain analytical functions $S_p(E)$ and $\Lambda_p(E)$. A Gaussian potential does not have these scaling properties.

In order to find an expression for $S_p(E)$ and $\Lambda_p(E)$ we have calculated periodic orbits, stability, action, and Maslov indexes for energy values in the interval $E\in[0.016,0.0247]$, $R=2.5$. We have approximated $S_p(E)$ and $\ln[\Lambda_p(E)]$ using polynomials of degree 5 in E for the real energy and used these functions as the analytical continuation into the complex energy plane.

In our model system we have chosen atomic units and consequently have $\hbar=1$. The semiclassical ζ function do not have any zeroes in the energy region $0.016<E<0.0247$ for $R=2.5$ if we use $\hbar=1$. If we choose $\hbar=0.05$ we find two resonances in this region, $E=0.0173-i0.00384$ and $E=0.0216-i0.00217$.

Changing $\hbar$ corresponds to choosing new parameters $\widetilde{m}$, $\widetilde{V}_0$, and $\widetilde{E}$, which fulfill the scaling conditions of the Hamiltonian for the three Gaussians.

$$\widetilde{m}\widetilde{V}_0=V_0, \quad \frac{\widetilde{E}}{\widetilde{V}_0}=\frac{E}{V_0} \tag{15}$$

and therefore do not change the dynamic and the stability of the system. If we set $\widetilde{m}=20$ we find $\widetilde{V}_0=-0.005$ and $\widetilde{E}=E/20$. By using $dS=p(dq/dt)dt$ we get the scaling of the action: $\widetilde{S}=S\widetilde{m}=S/0.05$. Because of this the ζ function remains the same if we use the new parameters in atomic units instead of the old parameters with $\hbar=0.05$. The resonances in the system with the new parameters are $\widetilde{E}=0.000865-i0.000192$ and $\widetilde{E}=0.00108,-i0.0001085$.

The resonances here are well within the energy interval without bifurcations and the imaginary part of the energy is quite small so we do not expect that including complex periodic orbits (ghost orbits) will significantly change the results. We have not calculated the resonances using quantum mechanics, but from calculations in other systems we expect the error to be relatively small.

IX. CONCLUSION

We have investigated a class of chaotic scattering Hamiltonian systems that is quite generic. The invariant structure in these systems has been determined by finding an asymptotic limit and then identified the same structure for the more complicated systems in a Poincaré plane. For some examples we have calculated periodic orbits and used these to find the classical escape time and the quantum mechanical resonances and demonstrated that this is possible for nontrivial systems. When the energy is very small for the scattering systems and for bounded systems of this type (double or triple wells and possibly the Hénon-Heiles potential), the structure of periodic orbits is very complicated and the methods applied here do not work directly. Further investigation is required for making classical and semiclassical calculations in these systems, but the methods for analyzing these have to be an extension of the methods used here.

ACKNOWLEDGMENTS

The authors would like to express their gratitude to Dieter Wintgen, who died a short time after having initiated this project. The authors thank John Briggs, Gernot Alber, Jan Michael Rost, Predrag Cvitanović, and Stephen Creagh for helpful discussions. K.T.H. is grateful to the Alexander von Humboldt foundation for financial support.

[1] H.A. Lorentz, Amst. Acad. **7**, 438 (1905).
[2] Ya.G. Sinai, Russ. Math. Surveys **25**, 137 (1970).
[3] B. Eckhardt, J. Phys. A **20**, 5971 (1987).
[4] P. Cvitanović and B. Eckhardt, Phys. Rev. Lett. **63**, 823 (1989).
[5] P. Gaspard and S.A. Rice, J. Chem. Phys. **90**, 2225 (1989); **90**, 2242 (1989).
[6] P. Gaspard and D. Alonso Ramirez, Phys. Rev. A **45**, 8383 (1992).
[7] P. Cvitanović, Niels Bohr Institute report (unpublished) (http://

www.nbi.dk/~predrag/QCcourse/).
[8] K.T. Hansen, Nonlinearity **6**, 753 (1993).
[9] S. Bleher, C. Grebogi, and E. Ott, Phys. Rev. Lett. **63**, 919 (1989).
[10] G. Troll and U. Smilansky, Physica D **35**, 34 (1989).
[11] G. Troll, Physica D **50**, 276 (1991).
[12] V. Daniels, M. Vallières, and J-M. Yuan, Chaos **3**, 475 (1993).
[13] M.S. Child, *Semiclassical Mechanics with Molecular Applications* (Clarendon, Oxford, 1991).
[14] M. Klein and A. Knauf, *Classical Planar Scattering by Coulombic Potentials*, Lecture Notes in Physics Vol. m13 (Springer-Verlag, Heidelberg, 1992).
[15] Jan M. Rost and Eric J. Heller, J. Phys. B. **27**, 1387 (1994).
[16] S. Smale, Bull. Am. Math. Soc. **73**, 747 (1967).
[17] P. Cvitanović and B. Eckhardt, Nonlinearity **6**, 277 (1993).
[18] P. Cvitanović, G.H. Gunaratne, and I. Procaccia, Phys. Rev. A **38**, 1503 (1988).
[19] K.T. Hansen, Phys. Rev. E **52**, 2388 (1995).
[20] H. Kantz and P. Grassberger, Physica D **17**, 75 (1985).
[21] K.T. Hansen, Ph.D. thesis, University of Oslo, 1993.
[22] R. Artuso, E. Aurell, and P. Cvitanović, Nonlinearity **3**, 325 (1990); **3**, 361 (1990).
[23] M.C. Gutzwiller, *Chaos in Classical and Quantum Mechanics* (Springer, New York, 1990).
[24] S.C. Creagh, J.M. Robbins, and R.G. Littlejohn, Phys. Rev. A **42**, 1907 (1990).
[25] H. Friedrich and D. Wintgen, Phys. Rep. **183**, 37 (1989).
[26] D. Wintgen, K. Richter, and G. Tanner, *CHAOS* **2**, 19 (1992).